Supplementary information

Supplementary Text 1: Model evaluation and validation

1.1 Model validation for the coupled land-atmosphere model

We used the coupled land-atmosphere model IPSL-CM (v6.0.10, an adaptation of IPSL-CM6A-LR)[1] for simulating the biophysical impacts of bioenergy crop cultivation. This coupled model integrates the ORCHIDEE-MICT-BIOENERGY land surface model[2,3] coupled with the LMDz (v6) atmospheric model[4,5]. The ORCHIDEE-MICT-BIOENERGY has been validated and shown to perform well in simulating global bioenergy crop yields[2,6–8]. The dynamic and physical processes of the atmosphere simulated by the coupled model have been well validated in previous studies[8–10]. The model outputs were generally consistent with stable-isotope-based transpiration observations, satellite-based surface radiation data, and surface energy fluxes derived from reanalysis data. The coupled IPSL-CM model was also able to reproduce the sensitivity of evapotranspiration to variations in leaf area index (LAI) and effectively capture the temporal fluctuations of surface energy fluxes[9,10]. The model performance on simulating albedo and evapotranspiration for both food crops and bioenergy crops were also fully evaluated[8] (detailed in Supplementary Text 1.3).

1.2 Validation for the carbon cycle

Model developments related to bioenergy crops were reported in detail in Li et al.[2]. After adding new processes (e.g., harvest) and adjusting parameters of photosynthesis, carbon allocation, phenology and harvest, the model can well reproduce the bioenergy crop yields at 196 locations with field measurement[2,6]. The new model version can also capture the biomass change with age increase for the woody bioenergy crops[2]. The SOC changes after converting other land use types to bioenergy crops were also validated against 57 field measurements compiled from 25 studies[7].

1.3 Validation for the biophysical variables

Validations of biophysical variables for food and bioenergy crops were also conducted in Wang et al.[8] and Li et al.[11]. Because a large fraction of bioenergy crop cultivation will occur on croplands (Supplementary Fig. 4), the key biophysical variables for both food and bioenergy crops need to be validated in order to accurately simulate the biophysical effects of land use change from food crop to bioenergy crop. Using FLUXNET data from 19 food crop sites, the model accurately represented the key biophysical variables of food crops with a strong agreement with observations[8]. Notably, the model reproduced observed seasonal variations in albedo and evapotranspiration with significant temporal correlations at most food crop sites[8]. Approximately two-thirds of monthly albedo observations were accurately predicted by the model. The biophysical variables for bioenergy crops were further validated against field measurements[8]. 241 field measurements of various bioenergy crop types were compiled, and after resolution aggregation, it resulted in 109 usable data points for evapotranspiration and 36 for albedo. The comparison between modeled and observed evapotranspiration showed a high degree of agreement, with 90 out of 109 evapotranspiration observations (approximately 83%) displaying error bars that intersected the 1:1 line. The model also captured seasonal variations in evapotranspiration effectively at most sites. The model also performed well in simulating albedo, with 28 out of 36 observations showing agreement within the error margins. Further validation was conducted through a comparison with satellite-based albedo observations for miscanthus and switchgrass across six different agricultural ecological zones in the U.S. from the MODIS[12]. This comparison confirmed that the simulated annual albedo values closely align with the observed values.

The hydrological variables for the coupled model with the bioenergy crop module were also validated[11], including comparison of model simulated precipitation against that from the Gridded Climatic Research Unit (CRU) Time-series (TS)[13] and Global Precipitation Climatology Centre (GPCC)[14] dataset for precipitation and the comparison of simulated evapotranspiration against that from the FLUXCOM[15] and GLEAM[16] datasets. The coupled model can generally capture the observed spatial patterns and magnitudes of precipitation and evapotranspiration, as well as the latitudinal variations and biome-specific trends[11]. Despite underestimation of precipitation in the Amazon basin and some regional discrepancies in evapotranspiration from the FLUXCOM and GLEAM datasets, the outputs from the coupled model are well within the observational ranges[11]. In addition, the runoff outputs from the coupled model were also consistent with the Global RUNoff ENSEMBLE (G-RUN ENSEMBLE) dataset[11,17].

Supplementary Text 2: Bioenergy crop cultivation maps

The two cultivation maps from 2015 to 2100 in the study are based on the bioenergy with carbon capture and storage (BECCS) scenarios from the integrated assessment model, MAgPIE[18] under the SSP2-2.6 (Shared Socio-economic Pathway 2 and Representative Concentration Pathway 2.6, the low-warming scenario) and SSP5-3.4 (SSP5 and RCP3.4, the overshoot scenario) pathways[19]. The maps were generated by harmonizing the historical patterns of cropland, pasture and grassland based on the Global Environmental History Database (HYDE 3.1)[20]. The low-warming BECCS scenario of MAgPIE employs BECCS as the only negative emission technology (NET), and thus there are no other NETs such as afforestation and reforestation[19]. These global cultivation maps show bioenergy crop cultivation in both CN and non-CN countries (Fig. 1). The total cultivation area under the low-warming scenario expands to 408 Mha in 2100 (352 Mha in the CN countries and 56 Mha in the non-CN countries). In the overshoot scenarios, the air temperature will increase rapidly and exceed the 2 °C warming target of Pairs Agreement in the first half of the 21st century, and NETs (mainly BECCS) will be widely deployed after 2040[19]. Hence, in the overshoot BECCS scenario, the total bioenergy crop cultivation area will reach 803 Mha in 2100 (645 Mha in the CN countries and 158 Mha in the non-CN countries). In line with the principle of cost minimization in MAgPIE, the bioenergy crop expansion area mainly comes from low vegetation such as cropland, pasture and grassland[18], and more forests will be converted into bioenergy crop cultivation under overshoot scenario than under low-warming scenario (Supplementary Fig. 2).

Supplementary Text 3: Estimating the biogeochemical effects

3.1 Response curves of carbon pools and calculation of net carbon-dioxide removal (CDR)

The offline simulation in this study used an improved version of the DGVM of ORCHIDEE-MICT[21]. This version incorporates processes related to the growth, ecology, and biomass harvest of bioenergy crops[2]. It includes four additional Plant Functional Types (PFTs) representing bioenergy crops: eucalypt, poplar-willow, miscanthus, and switchgrass. The parameterizations of the physiological processes, growth, and phenology of these bioenergy crop PFTs area based on extensive field observations[2]. This model version also includes a carbon pool for post-harvest biomass and a dynamic forest age-based harvest module specifically designed for woody bioenergy crops. The model has been validated and shown to perform well in simulating global bioenergy crop yields[2,6,8,7].

The response curves of carbon pools for 4 types of land use change (LUC) (from forest, grass, pasture and cropland to switchgrass) were obtained from the offline simulations, and then used to calculate the CDR under different bioenergy crop cultivation scenarios (see details in Wang et al.[7]). Specifically, the spin-up simulations were run to reach a steady state of the terrestrial ecosystem, where the atmospheric CO_2 concentration and land cover remained at the level of 1900, and a 20-year meteorological data cycle from 1901 to 1920 was used as the climate forcing data. Further, to simulate the historical carbon dynamics from 1901 to 2014, the historical transient climate data[22], varying atmospheric CO_2 concentration data (https://gml.noaa.gov/ccgg/trends/global.html) and annually updated PFT maps[23,24] were used to force the model.

In the next stage for simulations of idealized bioenergy crop cultivation, the atmospheric CO_2 concentration and land use type were fixed at the level of 2014, and the climate forcing data were cycled from 2007 to 2016[22]. In each idealized bioenergy crop cultivation simulation, one of the original vegetation types (such as cropland) would be converted to switchgrass cultivation in 2015 initially, and the model was then run to 2100 to obtain the response curves of different carbon pools. Therefore, each idealized bioenergy crop cultivation simulation could reflect the change of carbon pool caused by the conversion of one original land use type to switchgrass. We extracted the response curves at 0.5° × 0.5° grid level for different carbon pools including biomass, soil carbon, harvested bioenergy biomass, carbon capture and sequestration (CCS) processing loss. Their relationships follow:

$$\mathrm{CDR} = F_{\mathrm{CCS}} + F_{\mathrm{LUC}} \tag{1}$$

$$F_{\mathrm{CCS}} = \mathrm{Bioe}_{\mathrm{harvest}} - \mathrm{CCS}_{\mathrm{loss}} = \mathrm{Bioe}_{\mathrm{harvest}} \times \mathrm{CCS}_{\mathrm{efficiency}} \tag{2}$$

$$\mathrm{CCS}_{\mathrm{loss}} = \mathrm{Bioe}_{\mathrm{harvest}} \times \ (1 - \mathrm{CCS}_{\mathrm{efficiency}}) \tag{3}$$

$$F_{\mathrm{LUC}} = \Delta\mathrm{SOC}_{\mathrm{dec}} + \Delta\mathrm{SOC}_{\mathrm{acc}} + \Delta\mathrm{Bm}_{\mathrm{ori}} + \Delta\mathrm{Bm}_{\mathrm{bioe}} \tag{4}$$

In Supplementary Equation (1), CDR refers to the amount of net CO_2 removal, and F_{CCS} and F_{LUC} are the CCS flux and the carbon emissions caused by LUC. In Supplementary Equation (2), F_{CCS} represents the flux for permanent geological carbon capture and storage and is calculated by the product of harvested bioenergy crop biomass ($\mathrm{Bioe}_{\mathrm{harvest}}$) and CCS efficiency ($\mathrm{CCS}_{\mathrm{efficiency}}$). The $\mathrm{CCS}_{\mathrm{efficiency}}$ reported in literature varies from 44% to 90%[25–32], and here we took the median value (65%). In Supplementary Equation (3), $\mathrm{CCS}_{\mathrm{loss}}$ is the carbon loss in the process of CCS. In Supplementary Equation (4), F_{LUC} consists of the biomass loss of original vegetation type caused by LUC ($\Delta\mathrm{Bm}_{\mathrm{ori}}$), the decay of original soil organic carbon after LUC ($\Delta\mathrm{SOC}_{\mathrm{dec}}$), the biomass of bioenergy crop ($\Delta\mathrm{Bm}_{\mathrm{bioe}}$, including the unharvested biomass part), and the accumulation of soil carbon after LUC (ΔSOC_{acc})[2,7]. The positive or negative values stand for the land carbon sink or emission. Thus, the response curves at the grid cell scale were multiplied by the gridded cultivation areas to derive the CDR using a bookkeeping method. Contributions of the CN and non-CN countries to different components of CDR at the regional scale are shown in Supplementary Fig. 10.

3.2 Fertilization and the corresponding emissions

The CDR of bioenergy crop cultivation depends on its frequent harvest, which may result in a continuous loss of soil fertility because the nutrients (e.g., nitrogen) stored in harvested biomass would be removed from the ecosystem. It would lead to a reduction in crop productivity if not replenishing fertilizer to soils. In this study, we assumed that nitrogen fertilizers were applied to replenish the nitrogen loss during harvest based on the harvested biomass and the nitrogen concentrations in biomass[33,7] (Supplementary Table 1). A nitrogen use efficiency of 0.59 was used for the fertilizer application (Liu et al., 2010). The greenhouse gases (GHG) emissions (CO_2 equivalent, CO_2eq) during the production and transportation of nitrogen fertilizer were further calculated based on the GHG emission factors for nitrogen fertilizers in different regions of the world reported by FAO[34] (Supplementary Table 2). The N_2O emission during fertilizer application was also included using the emission factor (1.8% of nitrogen element)[35]. As a result, the GHG changes in this study contain the reduction of atmospheric CO_2 caused by CDR, the GHG emissions from nitrogen fertilizer production and transportation, and the N_2O emissions during nitrogen fertilizer application. Combined with the biomass production of bioenergy crop in each scenario, soil nitrogen loss caused by periodic harvests and the application amount of nitrogen fertilizer were estimated (Supplementary Table 1). The corresponding GHG emissions are shown in Supplementary Table 3.

3.3 Biogeochemical temperature change

In this study, we utilized the compact Earth System Model (OSCAR v3.1.1)[36,37] to analyze how the changes in atmospheric GHG concentrations induced by BECCS subsequently affected air temperature, the result is shown in Supplementary Fig. 11. We employed OSCAR (v3.1) to simulate air temperature changes resulting from the CDR processes associated with BECCS (Supplementary Text 3.1) and the GHG emissions associated with fertilization (Supplementary Text 3.2). To account for uncertainties inherent in such complex modeling, OSCAR incorporated a sampling approach by randomly selecting parameters from a diverse range originated from various complex Earth system models. Our study used a sample size of 2000. By aggregating the biogeochemical cooling effects in the 10 regions according to the OSCAR outputs (see the region division in Supplementary Fig. 3), we further calculated the global mean biogeochemical cooling effect. We also computed the impact of switchgrass cultivation in both CN and non-CN countries on changes in atmospheric CO_2 levels in 2100 (Supplementary Fig. 9). More details for simulating the biogeochemical effects can be found in Wang et al.[7].

Supplementary Text 4: Estimating the biophysical effects

4.1 Simulation based on the coupled model

We used the coupled land-atmosphere model IPSL-CM (v6.0.10, a modified version of IPSL-CM6A-LR)[1] to simulate the biophysical effects caused by bioenergy crop cultivation. This version of IPSL-CM contains the detailed ecological processes of bioenergy crops in the land model ORCHIDEE-MICT-BIOENERGY[2,3] and the atmospheric dynamics and physical processes in the atmosphere model LMDz (v6)[4,5]. The ocean and sea-ice models in the IPSL-CM are not activated in this study. Instead, the sea surface temperature and sea ice were prescribed using the climatological data from the Atmospheric Model Intercomparison Project (AMIP, www.pcmdi.llnl.gov/projects/amip) in our simulations. All coupled simulations were run for 50 years with the atmospheric CO_2 concentration same as that of 2014[23,24]. All the spatial resolutions of coupled simulation based on IPSL-CM in this study is 1.26° × 2.5° (latitude × longitude). In our study, the ORCHIDEE land surface model operates at a finer resolution (0.5° × 0.5°) than the coupled ORCHIDEE-LMDz model (1.26° × 2.5°). Therefore, the outputs of ORCHIDEE were aggregated to the resolution of the coupled model for further calculation when necessary.

The dynamic and physical processes of the atmosphere simulated by the coupled model have been well validated in previous studies[9,10,8]. The model outputs were generally consistent with stable-isotope-based transpiration observations, satellite-based surface radiation data, and surface energy fluxes derived from reanalysis data. The coupled IPSL-CM model was also able to reproduce the sensitivity of evapotranspiration to variations in leaf area index (LAI) and effectively capture the temporal fluctuations of surface energy fluxes[9,10]. The model performance on simulating albedo and evapotranspiration for both food crops and bioenergy crops were also fully evaluated[8].

For the scenarios of bioenergy crops cultivation, a total of 5 coupled simulations were conducted, including 4 bioenergy crop cultivation simulations and a reference scenario without bioenergy crop (Table 1). The 4 bioenergy crop cultivation simulations are switchgrass cultivation in the CN countries only and in both the CN and non-CN countries under the low-warming and overshoot scenarios, respectively. The reference scenario was based on the land cover in 2015 with fixed original vegetation types at the grid level. To assess the biophysical effects of switchgrass cultivation, we compared the results of the 4 bioenergy crop cultivation simulations to the reference simulation (Table 1). Note that the contribution of non-CN countries is calculated as the difference between the simulation with switchgrass cultivated in both CN and non-CN countries and the simulation with switchgrass cultivated only in the CN countries. All the bioenergy crop cultivation maps used in the simulations have various cultivation fractions in each grid cell, that is, bioenergy crops only cover a portion of each grid cell.

The main variables of vegetation growth such as leaf area index (LAI) and gross primary productivity (GPP), as well as variables closely related to energy balance, such as evapotranspiration (ET) and albedo, reached the steady state between the fifth and tenth year of simulation onset for switchgrass in the coupled simulations[8]. The results of the last ten years simulation were proved to be representative compared with that of the 36th to 50th year and 31st to 50th year[8]. Therefore, the biophysical effects of the bioenergy crop cultivation scenarios in this study were analyzed using the average results of the last decade of the 50-year simulation (i.e., 41st to 50th years). More details for simulating the biophysical effects can be found in Wang et al.[8]. Contributions of the CN and non-CN countries to biophysical air temperature change in each region are shown in Supplementary Fig. 12. It should be noted that there are marked differences between this study and the previous study by Wang et al.[8]: (1) Wang et al.[8] assumed that all countries would implement BECCS. In the current study, we ran additional simulations by assuming that bioenergy crops only cultivated in the CN countries and calculated the contribution of the non-CN countries. Such information cannot be derived from the previous simulations in Wang et al.[8] because of the strong non-linear processes related to the biophysical temperature changes. Therefore, the contributions of non-CN countries to the biophysical temperature change can only be deduced from the new simulations done in this study. These results also, for the first time, answered the key question that how much would be lost for global climate change mitigation if these countries decide not to adopt BECCS. (2) Wang et al.[8] only considered biophysical temperature changes induced by large-scale bioenergy crop cultivation, while this study also includes the biogeochemical temperature changes from the reduced atmospheric CO_2 concentrations due to the CDR of BECCS. The CDR of BECCS is a key concern in global climate negotiations and mitigation policymaking, but it was not analyzed in Wang et al.[8]. (3) Wang et al.[8] used only the low-warming scenarios with large-scale deployment of BECCS but didn't consider the overshoot scenarios. However, as the remaining carbon budget for the low-warming target getting smaller, the overshoot scenarios with deep decarbonization (e.g., large-scale BECCS deployment) after 2040 have drawn more attention. Therefore, this study also includes the overshoot scenarios, and the corresponding simulations were also newly added in this study.

Supplementary Text 5: Changes in atmospheric CO_2 concentrations and the biogeochemical temperature

In the low-warming scenario, cultivation of switchgrass results in a decrease of global atmospheric CO_2 concentration by 12 ppm (Supplementary Fig. 9). Specifically, cultivating switchgrass solely in the CN countries leads to a reduction of approximately 10 ppm in the global atmospheric CO_2 concentration (Supplementary Fig. 9). Further cultivation in the non-CN countries would lead to an additional 3 ppm reduction, accounting for 25% to the overall reduction (Supplementary Fig. 9). This proportion is higher than the proportion of their cultivation area (14%). In the overshoot scenario, the contributions to the CO_2 concentration reduction are 23 ppm (79%) and 6 ppm (21%) for the CN and non-CN countries, respectively. These proportions align with the proportions of cultivation areas (80% and 20%). Therefore, the contribution of the non-CN countries to the global total reduction in the atmospheric CO_2 concentration is relatively larger in the low-warming scenario than in the overshoot scenario. If switchgrass only cultivates in the CN countries, the global average biogeochemical cooling is -0.06 ± 0.07 °C and -0.14 ± 0.17 °C in the low-warming and overshoot scenarios (Supplementary Fig. 11). Further cultivation in the non-CN countries will lead to an extra biogeochemical cooling by 0.03 ± 0.02 °C and 0.05 ± 0.06 °C in the low-warming and overshoot scenarios (Supplementary Fig. 11).

Supplementary Text 6: Uncertainties

6.1 Uncertainties in CDR calculations

To account for the uncertainties inherent in the CDR estimates, we implemented a Monte Carlo simulation, performing 10,000 iterations to generate a range of possible outcomes. The analysis took into account the uncertainties in bioenergy yield estimations ($\sigma_{\mathrm{Bioeharvest}}$), SOC simulations ($\sigma_{\mathrm{SOC}}$) and CCS efficiency ($\sigma_{\mathrm{CCSefficiency}}$), each assumed to follow a normal distribution. For each iteration, values for bioenergy yields, SOC, and CCS efficiency were randomly sampled from their respective normal distributions.

For switchgrass yields simulated by the ORCHIDEE-MICT-BIOENERGY model, we employed the Percent Bias (PBIAS) as described by Moriasi et al.[38] and Li et al.[2] to estimate uncertainties in the yield prediction. This method quantifies the average tendency of the simulated biomass yields to be larger or lower than the observed yields. The average PBIAS value of 5% from Li et al.[2] was used to calculate $\sigma_{\mathrm{Bioeharvest}}$ as the uncertainty in the switchgrass yields.

For soil organic carbon (SOC) changes due to conversions of other land use types (forest, grassland, pasture, and cropland) to bioenergy crop cultivation, we quantified the uncertainty based on the model-observation comparisons from Wang et al.[7]. Field observations indicated an average increase of 18.5% increase in SOC after conversions of the four original land cover types to switchgrass cultivation, whereas the model predicted an average increase of 5.5%. Therefore, we took the model-observation difference (i.e., 13%) to calculate σ_{SOC}.

For the CCS efficiency, the reported range from literature is 44%~90%[25–32], which reflects the variability of CCS technologies and associated costs across different regions. This range was used to estimate $\sigma_{\mathrm{CCSefficiency}}$, and the median value (i.e., 65%) was used to calculate the main results.

Note that the belowground components in the calculation of biogeochemical effects include both changes in SOC (ΔSOC_{dec} and ΔSOC_{acc} in Supplementary Equation (4)) and permanent geological carbon capture and storage (F_{CCS} in Supplementary Equation (2)). In the low-warming scenario, the global total SOC change amounts to -9 ± 1.1

PgC globally, with CN countries and non-CN countries contributing -7.0 ± 0.9 (95% confidence interval, CI) PgC and -1.9 ± 0.2 PgC, respectively (Supplementary Fig. 14). In the overshoot scenario, the global total SOC change is -25.0 ± 3.3 PgC, with -19.0 ± 2.5 PgC and -6.0 ± 0.8 PgC from the CN and non-CN countries. On the other hand, F_{CCS} values are considerably higher, i.e., 72.0 ± 12.7 PgC and 150.0 ± 25.4 PgC in the low-warming and overshoot scenarios, respectively. The CN countries contribute 52.0 ± 10.2 PgC and 105.0 ± 20.8 PgC in the two scenarios, and the non-CN countries contribute 20.0 ± 2.5 PgC and 45.0 ± 4.6 PgC, respectively. Compared to permanent carbon storage, SOC is more sensitive the future climate change. Changes in future temperature and precipitation will affect the stability of SOC pools disproportionally, but the effects are not considered in our study, which may induce uncertainty. However, the magnitude of SOC change is much smaller than CCS, so this uncertainty is expected to have a minor impact on our results.

We integrated all the uncertainties above to calculate the overall uncertainty in CDR estimation (σ_{CDR}). Using the Monte Carlo simulation approach, we performed multiple iterations by sampling from the normal distributions of switchgrass yield, SOC, and CCS efficiency based on the mean value and the standard deviation (σ). In each iteration, we computed the total CDR by summing the contributions of switchgrass yields, SOC, and CCS efficiency (Supplementary Equations (1)-(4)). The results from all simulations were then aggregated to determine σ_{CDR}, which was subsequently converted into 95% confidence intervals (95% confidence interval, CI) by assuming a normal distribution (Supplementary Equation (5)). The results show that in the low-warming scenario, the total CDR in the non-CN countries is 9.1 ± 2.8 (95% CI) PgC, while in the overshoot scenario, it is 19.9 ± 5.2 PgC. The total CDR in the CN countries is 43.5 ± 11.5 and 77.6 ± 23.4 PgC in the low-warming and overshoot scenarios, respectively.

$$95\%\ \mathrm{CI} = \mathrm{total} \pm (1.96 \times \sigma_{\mathrm{CDR}}) \tag{5}$$

6.2 Uncertainties in air temperature change estimations

In the uncertainty estimation of biogeochemical temperature effects (σ_{bgc}), we incorporated variations in the OSCAR simulation outputs generated by 2000 times of parameter sampling, as detailed by Wang et al.[7]. The corresponding biogeochemical temperature change induced by switchgrass cultivation in the non-CN countries are -0.03 ± 0.04 °C in the low-warming scenario and -0.05 ± 0.06 °C in the overshoot scenarios. The changes induced by the CN countries are -0.06 ± 0.07 °C and -0.14 ± 0.17 °C, respectively.

The biophysical effects induced by bioenergy crop cultivation were simulated using the coupled land-atmosphere model IPSL-CM (v6.0.10, a modified version of IPSL-CM6A-LR)[1]. While this model can well represent the complex interactions between land use changes and climate dynamics, the estimation of uncertainties for biophysical effects remains challenging. To address this, we adopted a relative uncertainty measure based on a recent model intercomparison study that closely aligns with our scenarios[39]. We applied the relative uncertainty of 57%, which represents the inter-model variability, to estimate the uncertainty of biophysical effects (σ_{bph}) in our study. The estimated values of biophysical contributions by the non-CN countries are 0.02 ± 0.01°C in the low-warming scenario and 0.03 ± 0.02°C in the overshoot scenarios. The changes induced by the CN countries are 0.03 ± 0.02°C and -0.01 ± 0.01°C, respectively.

We integrated the uncertainties of biogeochemical and biophysical effects using the error propagation to calculate the overall uncertainty in the net air temperature change (σ_{net}, Supplementary Equation (6)). It resulted in a net air temperature change of -0.01 ± 0.04 °C in the low-warming scenario and -0.02 ± 0.06 °C in the overshoot scenarios contributed by the non-CN countries, compared to -0.03 ± 0.07 °C and -0.15 ± 0.17 °C by the CN countries, respectively (Supplementary Table 4).

$$\sigma_{\mathrm{net}} = \sqrt{\sigma_{\mathrm{bgc}}^2 + \sigma_{\mathrm{bph}}^2} \tag{6}$$

6.3 Possible delays in implementing bioenergy crop cultivation in different regions

In the main text, the contribution of the non-CN countries was quantified by assuming that both non-CN countries and CN countries implement bioenergy crop cultivation simultaneously. In reality there may be a delay in the BECCS implementation in the non-CN countries, which may lead to a decreased contribution from these countries towards the overall mitigation effort. To account for potential delays in bioenergy crop cultivation in the non-CN countries, we conducted a sensitivity test and assumed varying delayed years (Supplementary Fig. 13). For example, if the cultivation in the non-CN countries delays 20 years, the cumulative CDR would be reduced by 4 ± 1 PgC in the low-warming scenario and 12 ± 2 PgC in the overshoot scenario by 2100, and its proportion in the global total cumulative CDR would decrease by 7% and 11% (calculated based on the mean values), respectively, which is about half of the contribution of non-CN countries in the synchronous cultivation scenarios. Furthermore, even if the bioenergy crop cultivation is initiated by the CN countries, the timing of deployment in the non-CN countries may not be synchronized. Some non-CN countries may take action before others, but not all may follow. Nevertheless, delaying the bioenergy crop cultivation would result in a decrease in CDR and ultimately reduce the effectiveness of BECCS as a climate mitigation strategy.

For the CN countries, the achievement of carbon neutrality also remains uncertain, given the varying levels of social and economic development across different nations. Among the 136 CN countries, 69 countries, mostly in Africa and South and Central America, have carbon neutrality targets that are "under discussion" (Supplementary Fig. 1). These countries play a critical role in achieving global CDR targets due to the large areas of potential bioenergy crop cultivation and corresponding CDR in each scenario (Fig. 2b and c). However, the implementation of carbon-neutral policies in these regions faces potential conflicts between climate mitigation and local socio-economic development, such as the competition between bioenergy crops and food crops for land use. Moreover, social stability, external financial support, and technology transfer may also limit the ability of these countries to implement carbon neutrality policies[40,41]. These uncertainties regarding the likelihood and driving forces behind the adoption and implementation of carbon neutrality targets in these countries can impact estimates of achievable CDR and temperature change in the corresponding bioenergy crop cultivation scenarios.

6.4 Other uncertainties that are not accounted for

In this study, the amounts of CDR in different bioenergy crop cultivation scenarios were calculated using the response curves of various carbon pools derived from the offline simulations by ORCHIDEE-MICT-BIOENERGY. In the offline simulations, we used the cyclic meteorological data from 2007 to 2016 as the climate forcing data, and the atmospheric CO_2 concentration was also fixed at the level in the year of 2014, which ignores the impact of future climate change on the bioenergy crop biomass production.

In the low warming scenario, changes in future climate and the atmospheric CO_2 concentrations are moderate, and thus the influence on the growth of bioenergy crop and carbon pools is expected to be small[9]. But in the overshoot scenarios, the global temperature and atmospheric CO_2 concentrations are deemed to change dramatically due to massive emissions[42], resulting in a global warming of above 2°C in 2040. After 2040, the increased temperature is expected to be reduced through high-intensity NETs. As a result, bioenergy crop cultivation under the overshoot scenarios starting in 2040 is likely to be affected by changes in climate and atmospheric CO2 concentrations, which would alter the quantity of harvested biomass, land use change fluxes, and the corresponding biogeochemical temperature changes.

For other GHG emissions, we included the emissions of N_2O and other GHG from fertilization effect. However, the model used in this study does not yet include a complete representation of nitrogen cycle, and it cannot account for the possible limitations of nitrogen, phosphorus, and other nutrient elements on the growth of bioenergy crops. As a result, it may result in some consistency issues in estimating N_2O and other GHG emissions from fertilization. We only accounted for GHG emissions from fertilization because they are more related to the vegetation processes than other emissions from operational costs, biomass and CO_2 transportation, which may be implicitly included in the CCS efficiency. The uncertainty in the CCS efficiency has also been estimated and included in our analysis (Supplementary Text 6.1).

Supplementary Text 7: Simulation for eucalypt cultivation

Based on the same simulation setup as switchgrass, we also tested a woody bioenergy crop, eucalypt, to evaluate the climate mitigation potential of its cultivation. The representation of eucalypt in the model can be found in Li et al.[2] and Wang et al.[8]. Compared to switchgrass, eucalypt cultivation shows a higher CDR potential, primarily due to its higher biomass yields. The higher CDR then translates into more pronounced biogeochemical cooling effects, with a temperature change of -0.26 ± 0.20 °C in the low-warming scenario and -0.45 ± 0.38 °C in the overshoot scenario when cultivating eucalypt in both CN and non-CN countries (Supplementary Fig. 15).

In terms of biophysical effects, eucalypt cultivation results in very different temperature changes from switchgrass cultivation. Eucalypt cultivation in the CN countries contributes to a cooling effect of -0.01 ± 0.02 °C under the low-warming scenario but a warming effect of 0.01 ± 0.02 °C under the overshoot scenario (Supplementary Fig. 15). The contribution of further eucalypt cultivation in the non-CN countries is found to be negligible in the low-warming scenario (-0.0015 ± 0.0013 °C), but it shows a considerable biophysical cooling effect of -0.04 ± 0.03 °C in the overshoot scenario (Supplementary Fig. 15).

The overall contribution of non-CN countries is a reduction of the net air temperature by 0.05 ± 0.04 °C in the low-warming scenario and by 0.13 ± 0.11 °C in the overshoot scenario, respectively (Supplementary Fig. 15). This underscores the critical role that the non-CN countries play in global climate mitigation efforts.

Supplementary Text 8: Relationships of CDR and temperature change with cultivation area

There are complex interplays between the bioenergy crop cultivation area and the corresponding biophysical impacts on regional climate change, as reflected by the net air temperature change (Supplementary Fig. 16). The geographic distribution of CDR per cultivation area does not coincide with net cooling effects across the globe. It implies that while bioenergy crop implementation is aimed at mitigating global warming, the local temperature changes vary significantly. Regions with a higher CDR per cultivation area, such as central Africa and eastern South America, do not experience significant net cooling effects (Supplementary Fig. 16). In contrast, strong cooling effects are found in the high latitudes in North America and central Asia, but the CDR per cultivation area is low in these regions. It should be noted that the spatial pattern of net temperature changes is mainly controlled by the biophysical effects rather than the biogeochemical effects[8]. Compared to the biogeochemical cooling effects resulting from reduced atmospheric CO_2 concentration, which are rather homogenous, the biophysical effects are more regionally contrasted, controlled by changes in both local energy balance and atmospheric circulations. Contributions of the strong nonlinear processes related to the biophysical effects can only be determined by additional coupled simulations with specific simulation design.

To distinguish the biogeochemical effects and the biophysical effects of switchgrass cultivation, we plotted the relationships of biogeochemical and biophysical effects against CDR per cultivation area separately in grid cells with bioenergy crop cultivation (Supplementary Fig. 17, note that grid cells without bioenergy crop cultivation are excluded). Both biogeochemical and biophysical temperature changes show significantly negative correlations with CDR per cultivation area, indicating that CDR-effective regions have stronger temperature reduction. The stronger biophysical cooling effect in these regions is possibly due to the stronger evapotranspiration from the higher photosynthesis rates on these productive lands.

It should be noted that the biophysical temperature changes are specific to the scenarios where bioenergy crops are cultivated in all countries. These results are not applicable and cannot be extrapolated if some countries opt not to cultivate. The temperature changes in the cultivating countries cannot be assumed to remain unchanged, because the biophysical effects of bioenergy crop cultivation are influenced by many non-linear processes in the atmospheric circulation, which can cause teleconnection of temperature changes in other regions. Therefore, regional BECCS policy making should consider not only the local conditions but also the global efforts of implementing BECCS.

Supplementary Table 1 Nitrogen concentrations in aboveground biomass of switchgrass from published field data[33] and nitrogen fertilizer application amount from 2015 to 2100.

Bioenergy crop type	Nitrogen content of dry matters (g N kg^{-1})	Standard deviation of nitrogen content of dry matter (g N kg^{-1})	Nitrogen fertilizer applied in low-warming scenario (Pg N)	Nitrogen fertilizer applied in overshoot scenario (Pg N)
switchgrass	7.65	5.1	3.12	6.65

Supplementary Table 2 The GHG emission factors for the production and transportation of nitrogen fertilizer in different regions or continents in the world[34].

Region/Continent	Mean emission factor ($kg\ CO_2eq\ kg^{-1}\ N$)
Western Europe	5.62
Eurasia	6.87
South America	3.53
North America	4.00
Asia	6.92
Oceania	3.06

Supplementary Table 3 N_2O emissions caused by nitrogen fertilizer application and GHG emissions in the fertilizer production and transportation from 2005 to 2100.

Bioenergy crop type	N_2O emission in the low-warming scenario (Pg N)	N_2O emission in the overshoot scenario (Pg N)	GHG emission in the low-warming scenario (Pg C CO_2eq)	GHG emission in the overshoot scenario (Pg C CO_2eq)
switchgrass	0.06	0.12	3.83	8.61

Supplementary Table 4 Biophysical, biogeochemical and net effect of the CN and non-CN countries on temperature change under low-warming and overshoot scenarios. The uncertainties are shown as the 95% confidence intervals (CI). Note that the percentage of contribution is calculated based on the mean values of temperature change without accounting for the uncertainties.

	Low-warming scenario			**Overshoot scenario**		
	CN countries	non-CN countries	Global	CN countries	non-CN countries	Global
Biophysical (°C)	0.03±0.02	0.02±0.01	0.05±0.03	-0.01±0.01	0.03±0.02	0.02±0.01
Biogeochemical (°C)	-0.06±0.07	-0.03±0.04	-0.09±0.11	-0.14±0.17	-0.05±0.06	-0.19±0.19
Net ΔT (°C)	-0.03±0.07	-0.01±0.04	-0.04±0.11	-0.15±0.17	-0.02±0.06	-0.17±0.19
Contribution (%)		25%			12%	

Supplementary Fig. 1 Map of the CN countries and non-CN countries.

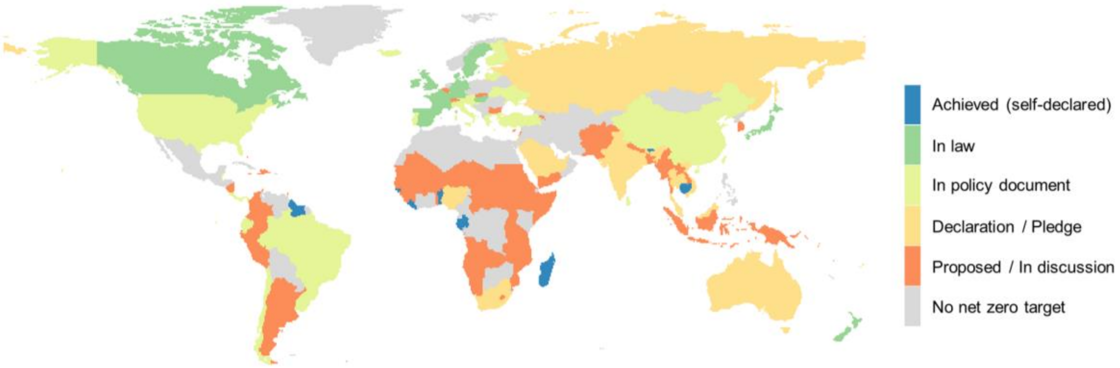

Supplementary Fig. 2 Spatial pattern and land source of bioenergy crop cultivation area under the low-warming (a) and overshoot (b) scenarios in this study. The pie charts show the proportion of the original vegetation types that are converted into bioenergy crop cultivation.

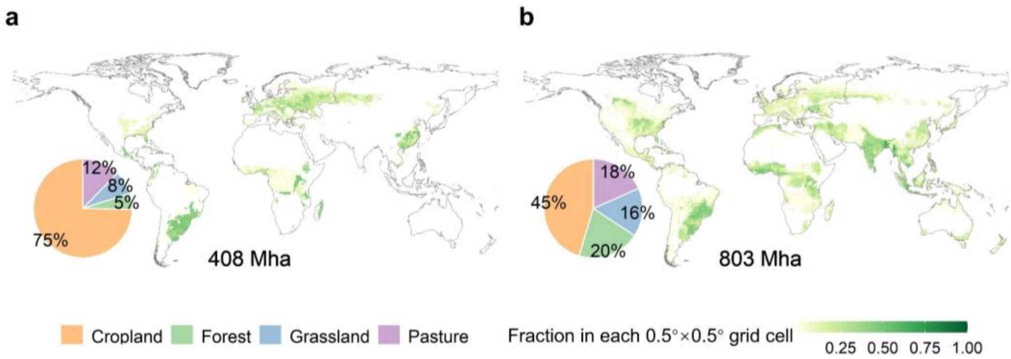

Supplementary Fig. 3 Region division used in this study.

Supplementary Fig. 4 Annual bioenergy cultivation area and the areas of original vegetation types being converted to bioenergy crop cultivation in the low-warming (a) and overshoot (b) scenarios.

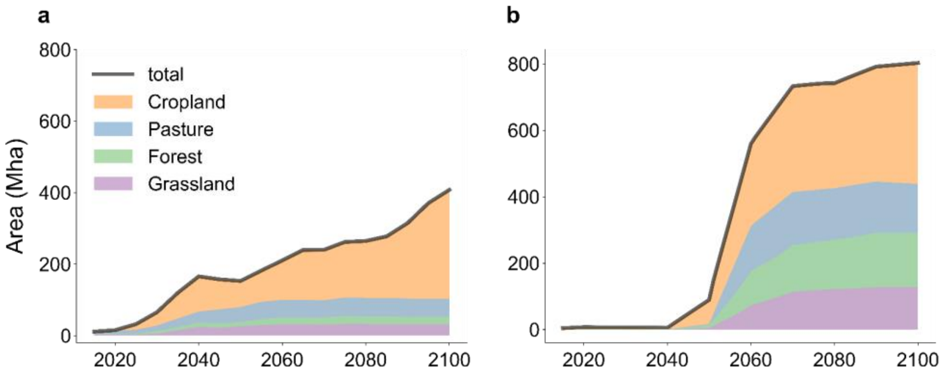

Supplementary Fig. 5 A schematic of methods for estimating biogeochemical and biophysical effects.

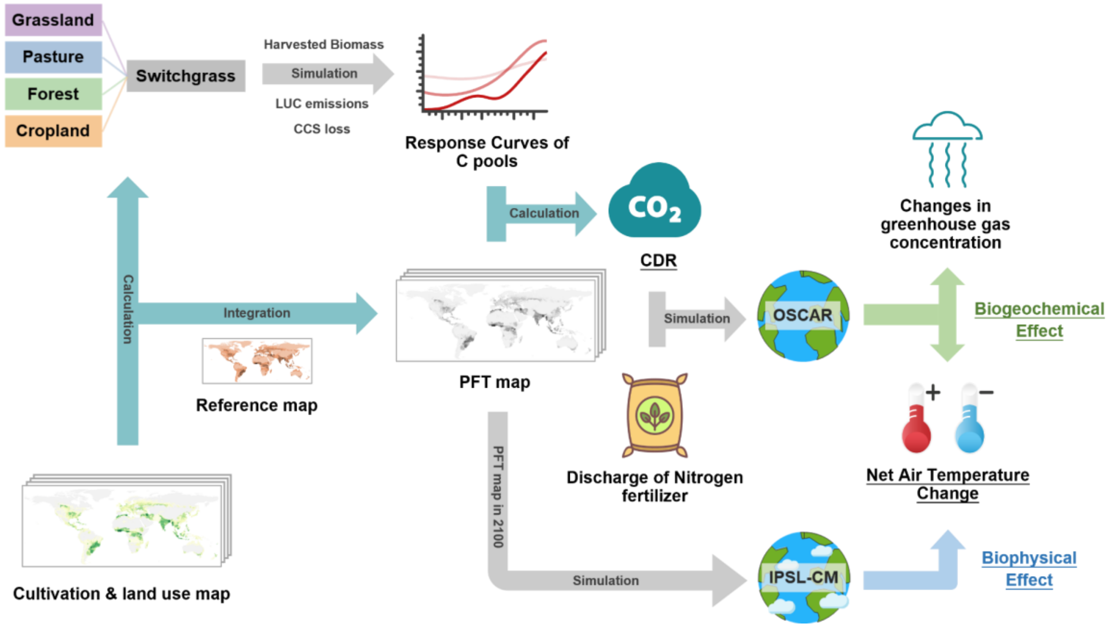

Supplementary Fig. 6 Contributions of the CN and non-CN countries to net carbon-dioxide removal (CDR) and biophysical air temperature change in the top ten non-CN countries with the largest cultivation area and the top ten CN countries with the maximum air temperature change under the low-warming (a and c) and overshoot (b and d) scenarios with switchgrass cultivation only in the CN countries and in all countries. Purple arrows refer to the biophysical air temperature change when cultivating switchgrass in the CN countries only, and green arrows indicate the biophysical air temperature changes after further cultivation in the non-CN countries. Pink dots indicate the amount of CDR in each country. DRC and CIV are the Democratic Republic of the Congo and the Republic of Côte d'Ivoire.

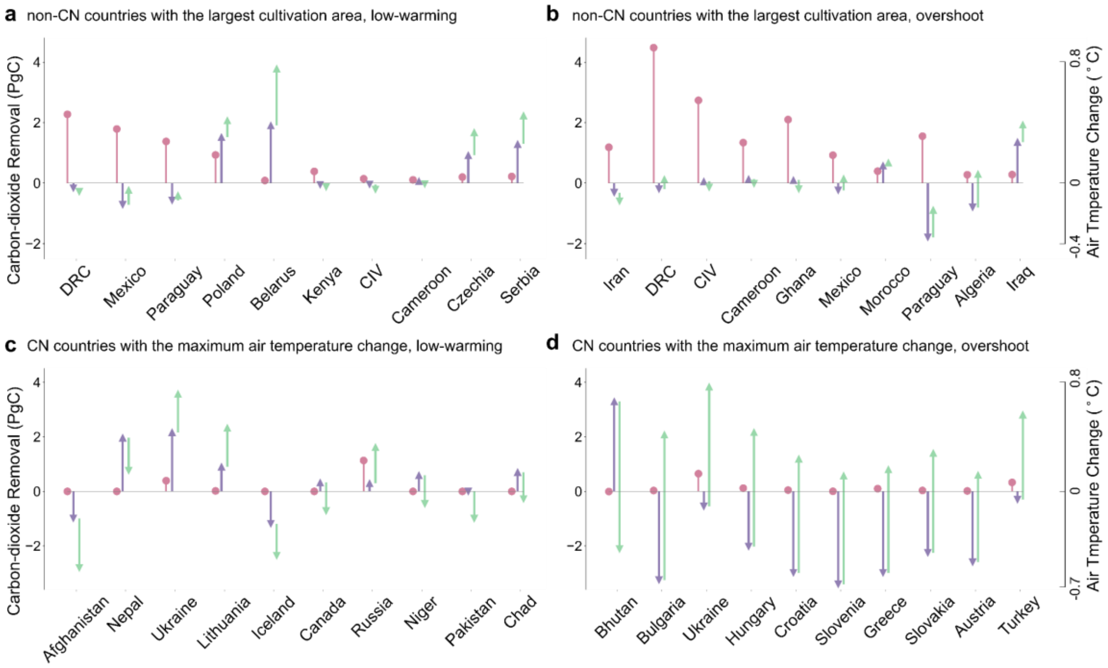

Supplementary Fig. 7 The cultivation area, net carbon-dioxide removal (CDR), biophysical air temperature change and net air temperature change in the top ten CN countries with the largest cultivation area under the low-warming (a) and overshoot (b) scenarios. Purple arrows refer to the biophysical air temperature change when cultivating switchgrass in the CN countries only, and green arrows indicate the biophysical air temperature changes after further cultivation in the non-CN countries. Blue arrows refer to the net air temperature change when cultivating switchgrass in the CN countries only, and green arrows indicate the net air temperature changes after further cultivation in the non-CN countries. Black and pink dots indicate the cultivation area and the amount of CDR in each country, respectively. USA is the United States of America.

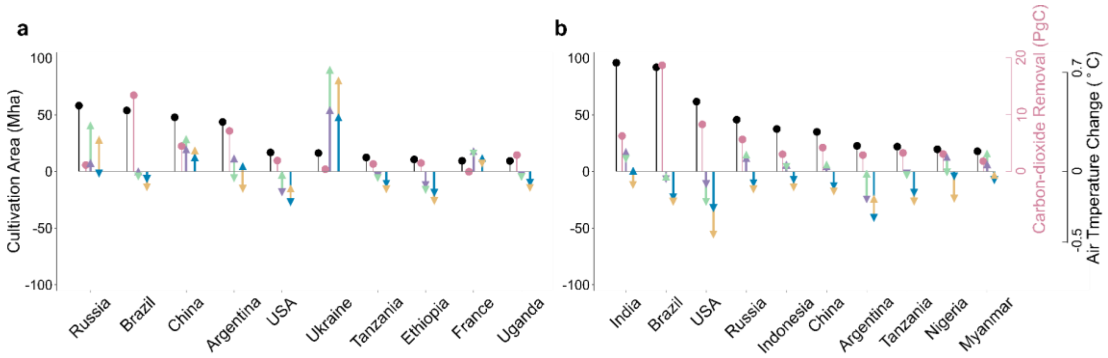

Supplementary Fig. 8 Biomass yields of switchgrass in the top ten non-CN countries with the largest cultivation area and the top ten CN countries with the maximum net air temperature change under the low-warming (a and c) and overshoot (b and d) scenarios. DRC and CIV are the Democratic Republic of the Congo and the Republic of Côte d'Ivoire.

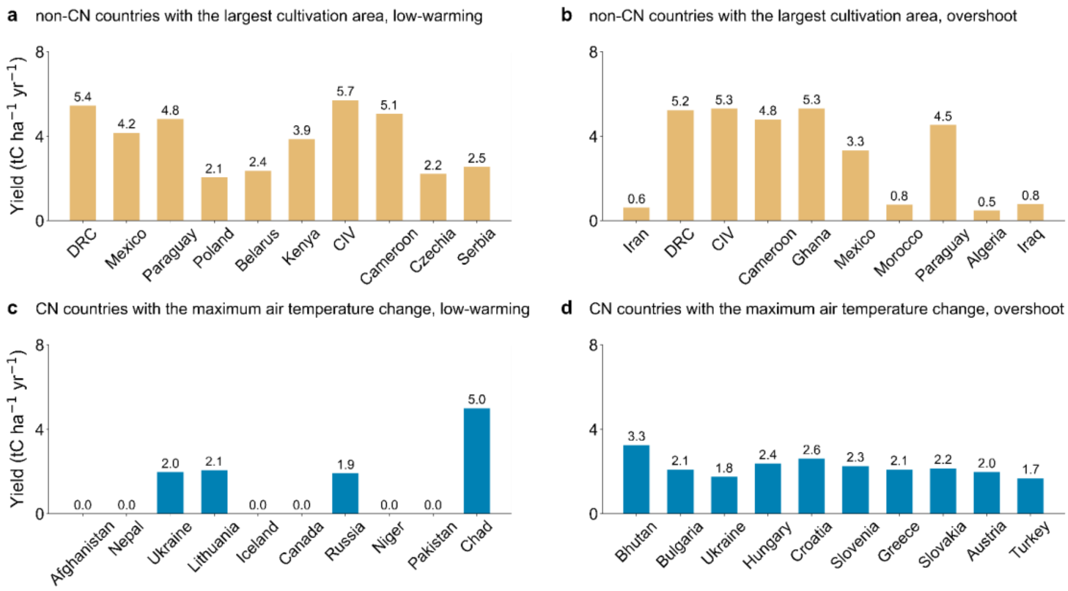

Supplementary Fig. 9 Contributions of the CN and non-CN countries to changes in the global CO_2 concentrations in the atmosphere from 2015 to 2100 under the low-warming and overshoot scenarios.

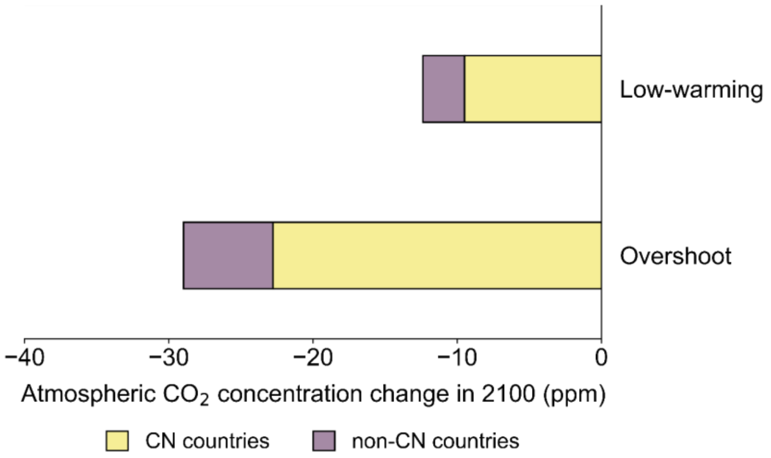

Supplementary Fig. 10 Contributions of the CN and non-CN countries to different components of net carbon-dioxide removal (CDR) in each region from 2015 to 2100 under the low-warming (a) and overshoot (b) scenarios. Darker and lighter bars are for the CN and non-CN countries, respectively. The red vertical lines stand for the total CDR in each region contributed by both the CN and non-CN countries (i.e., the sum of all bars).

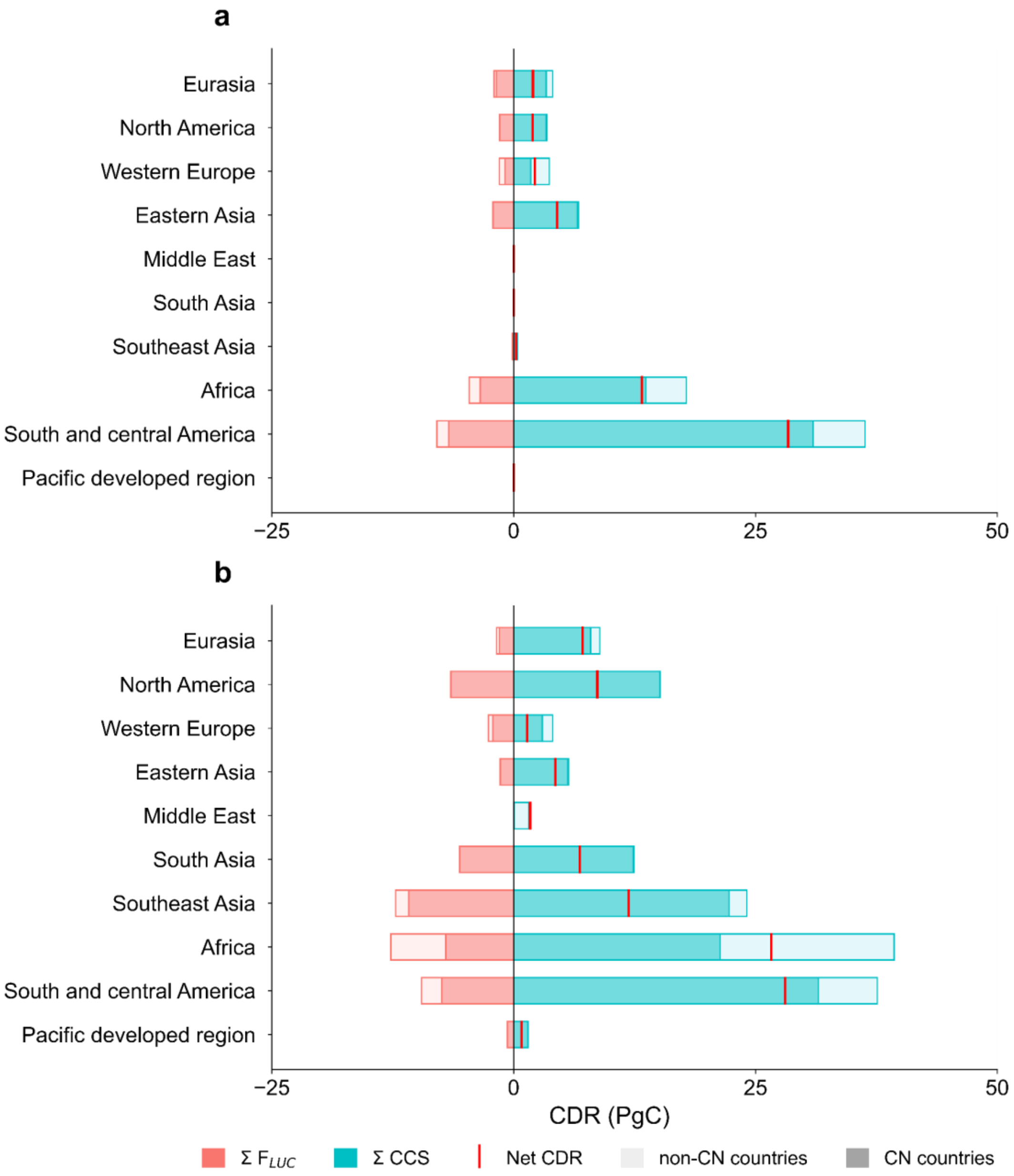

Supplementary Fig. 11 Contributions of the biogeochemical effects of CN and non-CN countries to the air temperature change under the low-warming (a) and overshoot (b) scenarios.

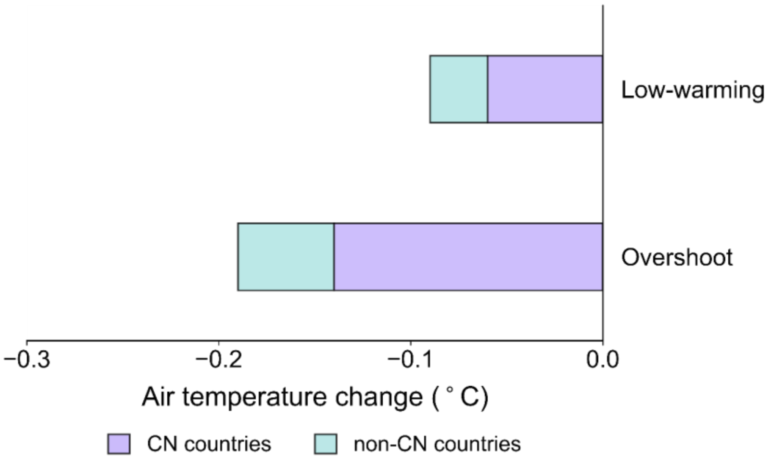

Supplementary Fig. 12 Contributions of the CN and non-CN countries to biophysical air temperature change in each region under the low-warming (a) and overshoot (b) scenarios. The black dots represent the biophysical air temperature change caused by the cultivation in both CN and non-CN countries.

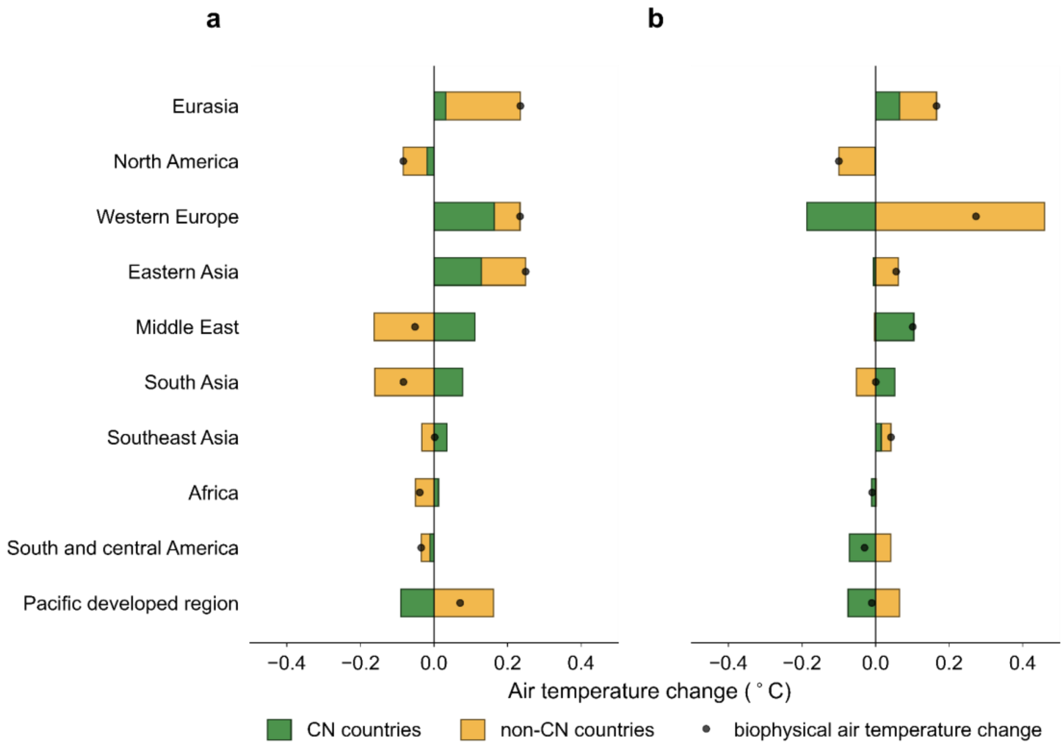

Supplementary Fig. 13 Impact of delayed implementation time of switchgrass cultivation in the non-CN countries on the CDR contribution of non-CN countries. The x-axis represents the delayed implementation years in the non-CN countries compared to the implementation year in the CN countries, and the y-axis refers to the CDR contribution of the non-CN countries to the global total CDR.

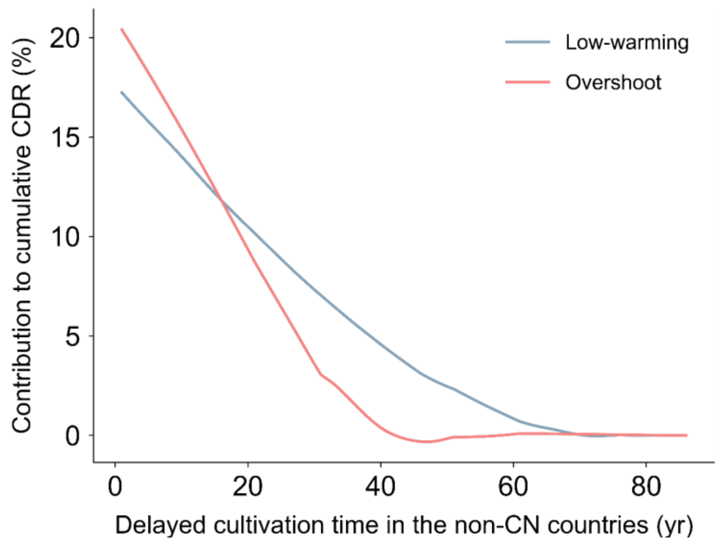

Supplementary Fig. 14 Contributions of different components to CDR induced by BECCS during 2015-2100 at the global scale under the low-warming and overshoot scenarios. Bars with different colors represent different components of CDR (**Supplementary Equations (1)-(4)**). Gray circles indicate the cumulative CDR at the global scale. Positive values indicate a removal of CO_2 from the atmosphere by convention.

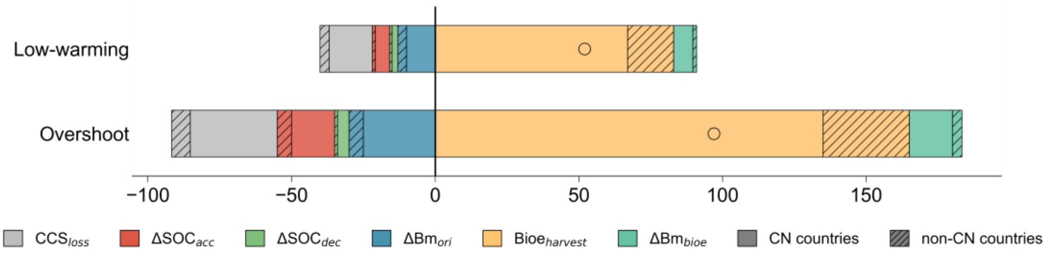

Supplementary Fig. 15 Contributions of the CN and non-CN countries to the global total net CDR, biogeochemical air temperature change (ΔT_{bgc}), biophysical air temperature change (ΔT_{bph}) and net air temperature change (ΔT_{net}) with switchgrass and eucalypt cultivation under the low-warming (a-d) and overshoot (e-h) scenarios. Blue bars represent changes when cultivating bioenergy crop in the CN countries only, and yellow bars represent further changes when cultivating bioenergy crop in both CN and non-CN countries. Arrows represent the directions of changes. Note that the yellow bar for ΔT_{bph} in (a) is invisible because the value (-0.0015 °C) is close to zero. Note that the scales of x-axis in **a-d** are different from those in **e-h**.

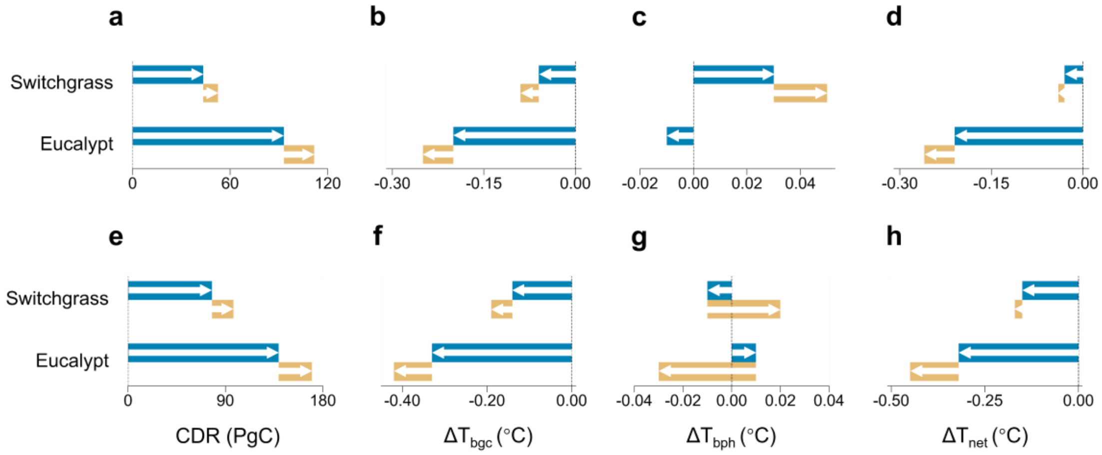

Supplementary Fig. 16 Spatial distribution of cumulative CDR per cultivation area during 2015-2100 and net air temperature (the sum of biogeochemical and biophysical temperature change) change induced by BECCS under the low-warming and overshoot scenarios.

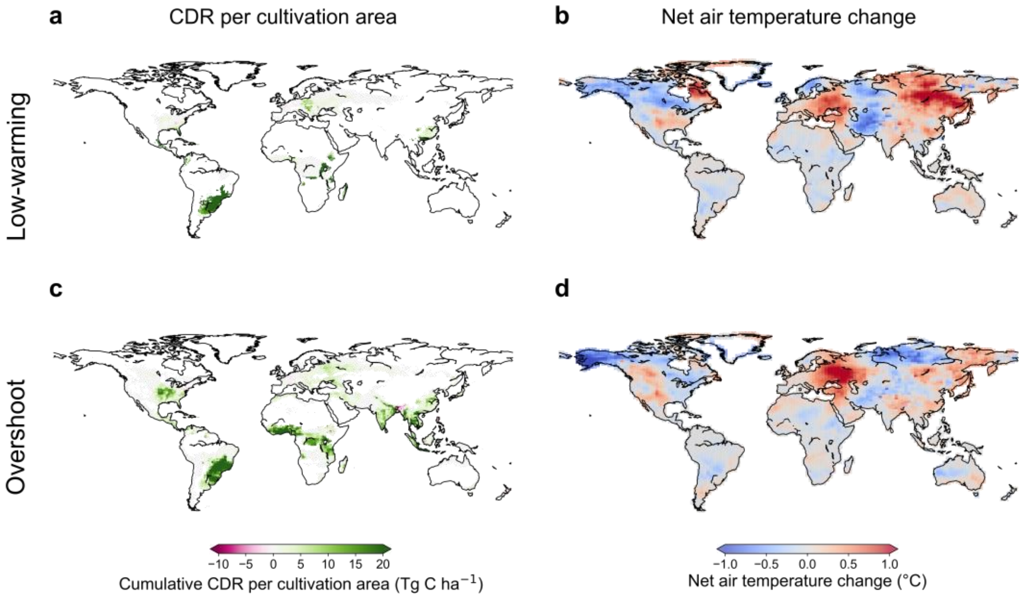

Supplementary Fig. 17 Relationship of biogeochemical and biophysical effects with CDR per cultivation area under the low-warming and overshoot scenarios. Blue dots represent the values in grid cells with valid data. The red lines represent the linear regression, and the shaded area is the 95% confidence interval.

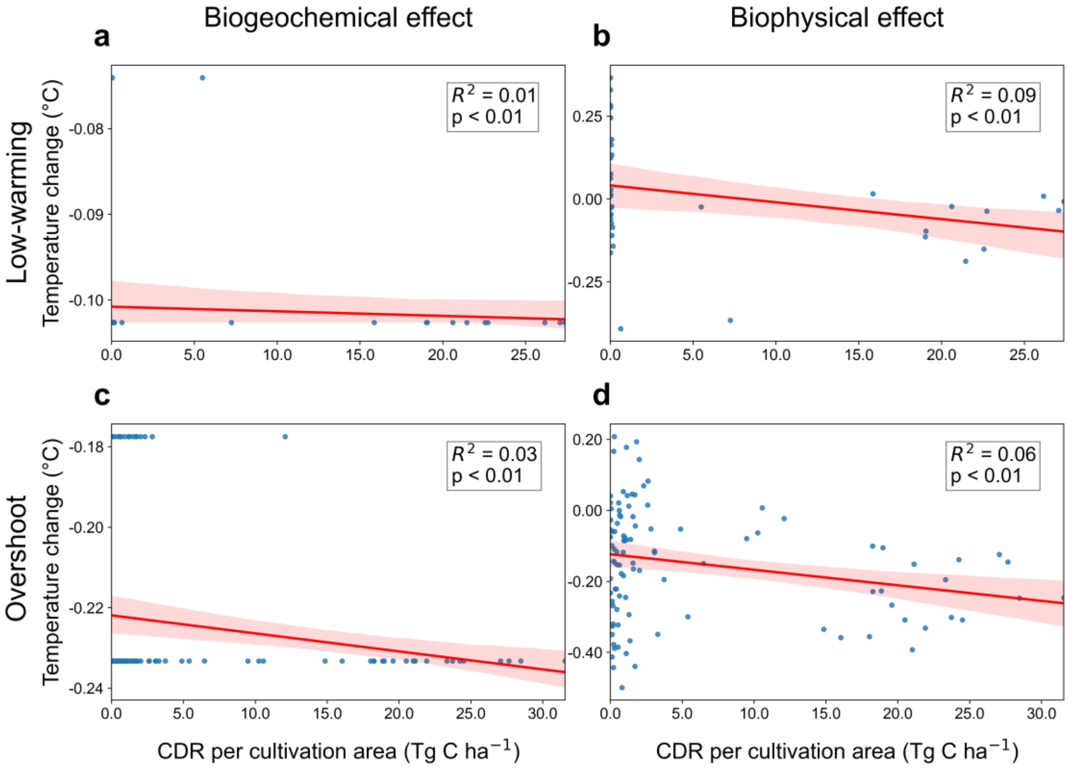

References

1. Boucher, O. *et al.* Presentation and Evaluation of the IPSL-CM6A-LR Climate Model. *J Adv Model Earth Syst* **12**, (2020).
2. Li, W. *et al.* ORCHIDEE-MICT-BIOENERGY: an attempt to represent the production of lignocellulosic crops for bioenergy in a global vegetation model. *Geosci. Model Dev.* **11**, 2249–2272 (2018).
3. Krinner, G. *et al.* A dynamic global vegetation model for studies of the coupled atmosphere-biosphere system. *Global Biogeochemical Cycles* **19**, 2003GB002199 (2005).
4. Hourdin, F. *et al.* The LMDZ4 general circulation model: climate performance and sensitivity to parametrized physics with emphasis on tropical convection. *Clim Dyn* **27**, 787–813 (2006).
5. Contoux, C., Ramstein, G. & Jost, A. Modelling the mid-Pliocene Warm Period climate with the IPSL coupled model and its atmospheric component LMDZ5A. *Geosci. Model Dev.* **5**, 903–917 (2012).
6. Li, W., Ciais, P., Makowski, D. & Peng, S. A global yield dataset for major lignocellulosic bioenergy crops based on field measurements. *Sci Data* **5**, 180169 (2018).
7. Wang, J. *et al.* Temperature Changes Induced by Biogeochemical and Biophysical Effects of Bioenergy Crop Cultivation. *Environ. Sci. Technol.* **57**, 2474–2483 (2023).
8. Wang, J. *et al.* Global cooling induced by biophysical effects of bioenergy crop cultivation. *Nat Commun* **12**, 7255 (2021).
9. Li, Y., Piao, S., Chen, A., Ciais, P. & Li, L. Z. X. Local and teleconnected temperature effects of afforestation and vegetation greening in China. *National Science Review* **7**, 897–912 (2020).
10. Zeng, Z. *et al.* Climate mitigation from vegetation biophysical feedbacks during the past three decades. *Nature Clim Change* **7**, 432–436 (2017).
11. Li, Z. *et al.* Increased precipitation over land due to climate feedback of large-scale bioenergy cultivation. *Nat Commun* **14**, 4096 (2023).
12. Cai, H. *et al.* Consideration of land use change-induced surface albedo effects in life-cycle analysis of biofuels. *Energy Environ. Sci.* **9**, 2855–2867 (2016).
13. Harris, I., Osborn, T. J., Jones, P. & Lister, D. Version 4 of the CRU TS monthly high-resolution gridded multivariate climate dataset. *Sci Data* **7**, 109 (2020).
14. Schneider, U., Becker, A., Finger, P., Rustemeier, E. & Ziese, M. GPCC Full Data Monthly Version 2020 at 1.0°: Monthly Land-Surface Precipitation from Rain-Gauges built on GTS-based and Historic Data: Gridded Monthly Totals. 5 MB-300 MB per gzip compressed NetCDF file [object Object] https://doi.org/10.5676/DWD_GPCC/FD_M_V2020_100 (2020).
15. Jung, M. *et al.* The FLUXCOM ensemble of global land-atmosphere energy fluxes. *Sci Data* **6**, 74 (2019).
16. Martens, B. *et al.* GLEAM v3: satellite-based land evaporation and root-zone soil moisture. Preprint at https://doi.org/10.5194/gmd-2016-162 (2016).
17. Ghiggi, G., Humphrey, V., Seneviratne, S. I. & Gudmundsson, L. G-RUN ENSEMBLE: A Multi-Forcing Observation-Based Global Runoff Reanalysis. *Water Resources Research* **57**, e2020WR028787 (2021).
18. Popp, A. *et al.* Land-use transition for bioenergy and climate stabilization: model comparison of drivers, impacts and interactions with other land use based mitigation options. *Climatic*

Change **123**, 495–509 (2014).
19. Hurtt, G. C. *et al.* Harmonization of global land use change and management for the period 850–2100 (LUH2) for CMIP6. *Geosci. Model Dev.* **13**, 5425–5464 (2020).
20. Klein, D. *et al.* The value of bioenergy in low stabilization scenarios: an assessment using REMIND-MAgPIE. *Climatic Change* **123**, 705–718 (2014).
21. Guimberteau, M. *et al.* ORCHIDEE-MICT (v8.4.1), a land surface model for the high latitudes: model description and validation. *Geosci. Model Dev.* **11**, 121–163 (2018).
22. Viovy, N. CRUNCEP Version 7 - Atmospheric Forcing Data for the Community Land Model. in (2018).
23. Sitch, S. A. *et al.* Recent trends and drivers of regional sources and sinks of carbon dioxide. *Biogeosciences* **12**, 653–679 (2015).
24. Peng, S. *et al.* Sensitivity of land use change emission estimates to historical land use and land cover mapping. *Global Biogeochemical Cycles* **31**, 626–643 (2017).
25. Smith, L. J. & Torn, M. S. Ecological limits to terrestrial biological carbon dioxide removal. *Climatic Change* **118**, 89–103 (2013).
26. Boysen, L. R. *et al.* The limits to global-warming mitigation by terrestrial carbon removal. *Earth's Future* **5**, (2017).
27. Read, P. Biosphere carbon stock management: addressing the threat of abrupt climate change in the next few decades: an editorial essay. *Climatic Change* **87**, 305–320 (2008).
28. Bui, M. *et al.* Carbon capture and storage (CCS): the way forward. *Energy Environ. Sci.* **11**, 1062–1176 (2018).
29. Rhodes, J. S. & Keith, D. W. Engineering economic analysis of biomass IGCC with carbon capture and storage. *Biomass and Bioenergy* **29**, 440–450 (2005).
30. Kuramochi, T., Ramírez, A. R., Turkenburg, W. & Faaij, A. P. C. Comparative assessment of CO2 capture technologies for carbon-intensive industrial processes. *Progress in Energy and Combustion Science* **38**, 87–112 (2012).
31. Koornneef, J., Keulen, T. van, Faaij, A. P. C. & Turkenburg, W. Life cycle assessment of a pulverized coal power plant with post-combustion capture, transport and storage of CO2. *International Journal of Greenhouse Gas Control* **2**, 448–467 (2008).
32. Hanssen, S. V. *et al.* The climate change mitigation potential of bioenergy with carbon capture and storage. *Nat. Clim. Chang.* **10**, 1023–1029 (2020).
33. Li, W. *et al.* Bioenergy Crops for Low Warming Targets Require Half of the Present Agricultural Fertilizer Use. *Environmental science & technology* (2021).
34. FAO. Global database of GHG emissions related to feed crops. (2017).
35. Tian, D. & Niu, S. A global analysis of soil acidification caused by nitrogen addition. *Environ. Res. Lett.* **10**, 024019 (2015).
36. Gasser, T. *et al.* The compact Earth system model OSCAR v2.2: description and first results. *Geosci. Model Dev.* **10**, 271–319 (2017).
37. Arneth, A., Schurgers, G., Hickler, T. & Miller, P. A. Effects of species composition, land surface cover, CO2 concentration and climate on isoprene emissions from European forests. *Plant Biol (Stuttg)* **10**, 150–162 (2008).
38. D. N. Moriasi *et al.* Model Evaluation Guidelines for Systematic Quantification of Accuracy in Watershed Simulations. *Transactions of the ASABE* **50**, 885–900 (2007).
39. He, M. *et al.* Amplified warming from physiological responses to carbon dioxide reduces the

potential of vegetation for climate change mitigation. *Commun Earth Environ* **3**, 160 (2022).
40. Dong, F. *et al.* How green technology innovation affects carbon emission efficiency: evidence from developed countries proposing carbon neutrality targets. *Environmental Science and Pollution Research* **29**, 35780–35799 (2022).
41. Wei, Y.-M. *et al.* Policy and Management of Carbon Peaking and Carbon Neutrality: A Literature Review. *Engineering* **14**, 52–63 (2022).
42. Kriegler, E. *et al.* Fossil-fueled development (SSP5): An energy and resource intensive scenario for the 21st century. *Global Environmental Change* **42**, 297–315 (2017).